Available online at www.sciencedirect.com

ScienceDirect

Procedia Structural Integrity 61 (2024) 214–223

Structural Integrity Procedia

www.elsevier.com/locate/procedia

3rd International Workshop on Plasticity, Damage and Fracture of Engineering Materials (IWPDF 2023)

Thermomechanical modeling of the shearing process during fine blanking of quenched and tempered steel

Frank Schweinshaupt[a,*], Thomas Stoel[a], Martina Müller[a], Tim Herrig[a], Thomas Bergs[a,b]

[a]*Manufacturing Technology Institute – MTI of RWTH Aachen University, 52074 Aachen, Germany*
[b]*Fraunhofer Institute for Production Technology IPT, 52074 Aachen, Germany*

Abstract

In order to develop an alloy design for fine blanking of deformation mechanism-based sheet metal materials such as high manganese steel, knowledge of the temperature during the shearing process is required. Thermomechanical modeling of shear zone temperature requires consideration of contact heat transfer, which depends on stress state as well as temperature. This paper deals with a methodology for calibrating the contact heat transfer coefficient during fine blanking using indirect temperature measurements. For this purpose, a thermomechanically coupled finite element (FE) model was designed considering thermoviscoplasticity, temperature-dependent physical and thermophysical parameters as well as a steady-state calibrated contact heat transfer coefficient. Experimental fine blanking tests were carried out to validate the model using force, die roll and thermography measurements based on varied blanking velocities. The thermomechanically coupled FE modeling showed a sufficiently accurate correspondence regarding the experimentally determined blanking force, die roll as well as sheared surface temperature. Thermographically determined sheared surface temperatures allowed calibration of locally different contact heat transfer coefficients as a simplified approach under steady-state conditions.

© 2024 The Authors. Published by Elsevier B.V.
This is an open access article under the CC BY-NC-ND license (https://creativecommons.org/licenses/by-nc-nd/4.0)
Peer-review under responsibility of the scientific committee of IWPDF 2023 Chairman

Keywords: Fine blanking; Thermoviscoplastic modeling; Thermographic measurement; Contact heat transfer; Shear zone temperature

1. Introduction

The characteristic of fine blanking causes thermomechanically induced heat dissipation in the shear zone, which is influenced by the process parameters. The specific fine blanking tool and process parameters result in superimposed compressive stress in the shear zone and lead to plastic flow along the shearing path, which is associated with heat

* Corresponding author. Tel.: +49-241-8024977.
E-mail address: f.schweinshaupt@mti.rwth-aachen.de

2452-3216 © 2024 The Authors. Published by ELSEVIER B.V.
This is an open access article under the CC BY-NC-ND license (https://creativecommons.org/licenses/by-nc-nd/4.0)
Peer-review under responsibility of the scientific committee of IWPDF 2023 Chairman
10.1016/j.prostr.2024.06.028

dissipation. Depending on the load spectrum, the dissipated heat accumulates in the shear zone and causes a temperature rise along the sheared path. Demmel et al. (2015) conducted experimental temperature measurements during shearing of 6 mm thick micro-alloyed fine grain steel with small die clearance. With an increase in blanking velocity from 10 to 70 mm/s, a maximum temperature of approx. 270 °C was determined around the punch edges. The process parameter-dependent shear zone heating has an influence on the activation of the deformation mechanisms during fine blanking of high manganese steel and thus on the realization of a high sheared surface hardening (Babaei et al. (2023)). The development of an alloy design for fine blanking of high manganese steel requires numerical modeling of the shear zone temperature, considering parameters with thermomechanical influence. Material modeling in shearing regarding the flow behavior as well as ductile fracture criterion has been investigated in several scientific studies (Kolhatkar and Pandey (2023)). For modeling the temperature- and strain rate-dependent plastic flow occurring in the shear zone, thermoviscoplastic flow curve models that consider strain hardening are suitable (Joun et al. (2022)). Ductile fracture models commonly used in fine blanking are Cockcroft-Latham and Oyane. Wai Myint et al. (2018) investigated the critical fracture criteria for Cockcroft-Latham normalized and Oyane depending on the die clearance during fine blanking and showed a sufficiently accurate representation of the clean-shear area for both criteria.

For an accurate numerical modeling of the shear zone temperature, which depends on the heat equalization processes, a determination of the thermophysical parameters of all contact partners is necessary, which results in a high experimental effort. For example, Kim et al. (2007) investigated the thermal influence on fine blanking based on thermographic measurements and numerical analysis. However, the blanked part temperatures determined experimentally and numerically showed a difference of approx. 20 °C. Rosochowska et al. (2003) analyzed the influence of high contact normal stress up to 450 MPa as well as the arithmetical mean roughness Ra on contact heat transfer at temperatures of 200 and 300 °C. With decreasing roughness and increasing contact normal stress, the contact heat transfer coefficient increased significantly. Since high contact normal stresses occur at increased temperatures during fine blanking in the shear zone, an influence of the modeled contact heat transfer in the area of the die and punch edges on the numerical shear zone temperature is to be expected. In order to thermomechanically model the shearing process during fine blanking considering the contact conditions, a methodology for calibrating locally different steady-state contact heat transfers was investigated in the present work. The methodology was derived by means of an experimental investigation of the sheared surface temperature based on thermographic measurements during fine blanking of quenched and tempered steel 42CrMo4+AC (AISI 4140). Based on determined temperature, force and die roll measurements, a validation of the thermomechanically coupled model as well as an analysis of the shearing process at varied blanking velocities was carried out.

2. Experimental setup and numerical modeling for fine blanking

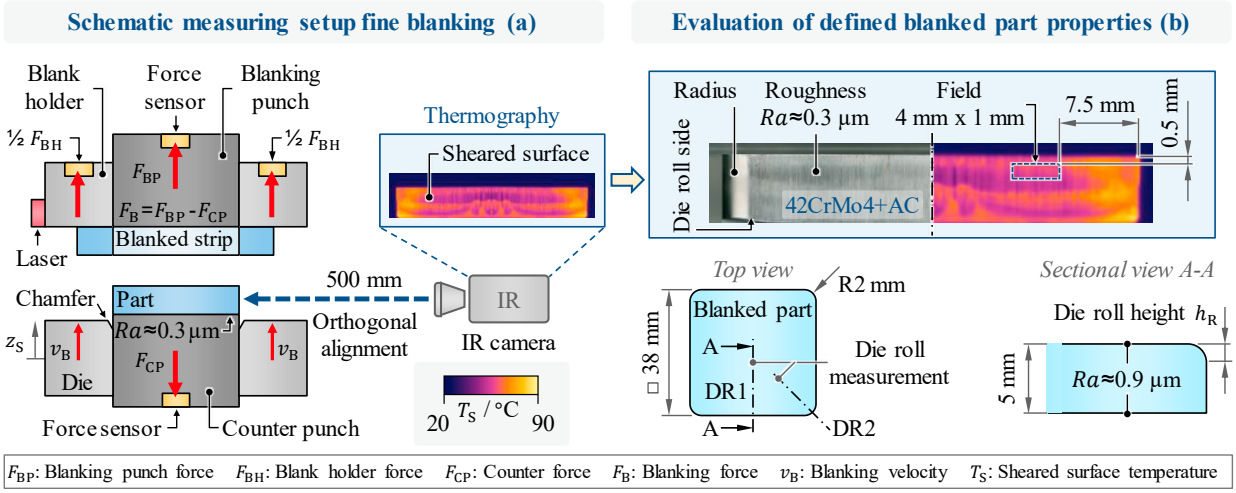


Fig. 1: Thermomechanical measuring setup for fine blanking (a) and evaluation of defined fine blanked part properties (b)

The fine blanking experiments were performed on a modular designed tool, which is instrumented with force sensors to measure the process forces as well as laser displacement sensors to measure the shearing path z_S (Fig. 1a). The square blanked part geometry used was designed in the tool in such a way that an infrared camera (IR camera) can be aligned at a defined distance orthogonal to the sheared surface. Thermographic measurement of the sheared surface temperature was performed with a *FLIR X6580SC* IR camera using two overlapping temperature ranges between 10 and 220 °C at a frame rate of 353 Hz. To determine the sheared surface temperature, a measuring field 4 mm long and 1 mm high was positioned just below the blanked edge opposite the die roll side. Since due to symmetry reasons one quarter of the blanked part geometry is sufficient for numerical modeling, the measuring field was aligned centrally on the right half surface (Fig. 1b). For the evaluation of the sheared surface temperature, the emissivity was determined in a separate measurement setup using a heating plate, thermocouple measurement on the blanked part and IR camera in a temperature range from 35 to 200 °C. To determine the die roll, the fine blanked parts were polygonized using a *GOM ATOS Core 3D* scanner and a software-based target-actual comparison was performed using a CAD model by means of *GOM Inspect Suite*. For this purpose, the height differences at the positions DR1 and DR2 marked in Fig. 1b were measured in a 2D plot using sectional planes and evaluated script-based. The fine blanking experiments were carried out on a *Feintool XFT 2500 speed* servomechanical fine blanking press with roller levelled and cut to length blanks from a coil of quenched and tempered steel 42CrMo4+AC (1.7225 or AISI 4140) with a sheet thickness of 5 mm. The sheet metal material was annealed to achieve spheroidized carbides (+AC).

Table 1: Mechanical properties sheet metal material as well as process and tool parameters

Mechanical properties 42CrMo4+AC		Process parameters		Tool parameters	
Yield strength	316 MPa	Blanking velocity v_B	15 / 45 / 75 mm/s	Die clearance	20 µm
Ultimate tensile strength	478 MPa	Blank holder force F_{BH}	310 kN	Die chamfer angle	35°
Elongation at fracture A_{80}	29%	Counter force F_{CP}	145 kN	Die chamfer height	0.3 mm

The blanking punch and die were manufactured from *Böhler S390* powder metallurgical high speed steel with a hardness of 65 HRC and provided with the *Platit FeinAl* coating (AlCrN-based nanolayer coating) tailored to fine blanking. Fine blanking was carried out without vee-ring using chlorine-free lubricant *Holifa VP1150/200*. The fine blanking experiments were conducted with varied blanking velocities of 15, 45 and 75 mm/s and repeated five times for each test parameter to average the measurement results. Table 1 shows the mechanical properties of the sheet metal material as well as the relevant process and tool parameters.

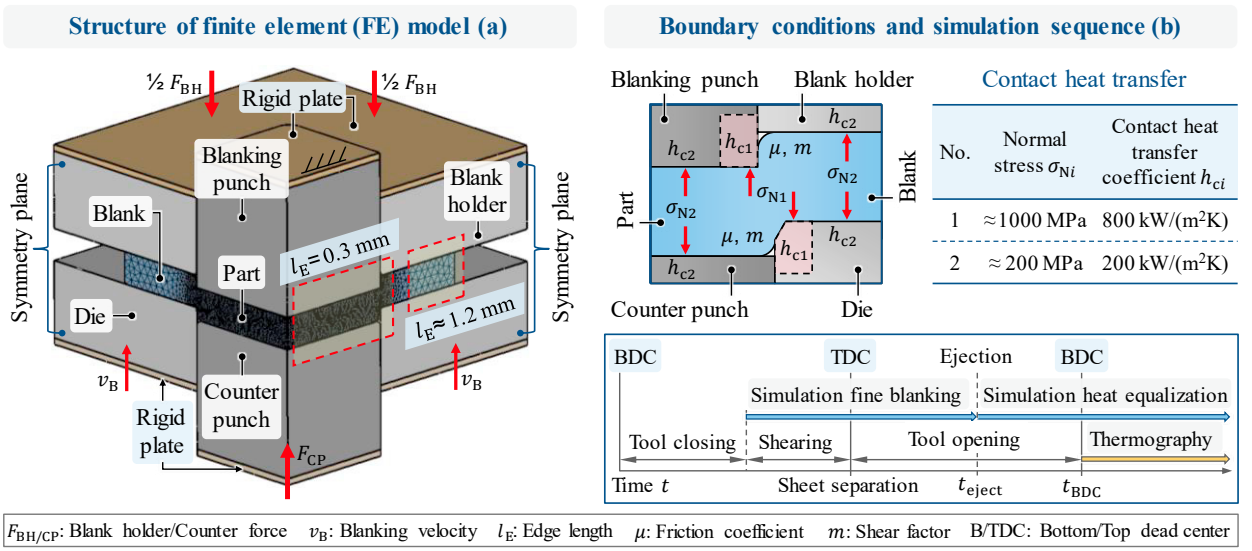


Fig. 2: Structure of FE model for fine blanking (a) with boundary conditions and assignment of simulation sequence to process (b)

Analogous to the setup used for fine blanking experiments, a finite element (FE) model was designed for numerical analysis in Forge NxT 3.2 software, which uses an implicit solver for calculation. Taking advantage of the symmetry, a quarter of the blanked part geometry was modeled (Fig. 2a). All modeled tool elements have been connected to rigid plates for force or movement initiation as well as fixed clamping. The process forces are applied to the blank holder and counter punch with the parameters used in the experiments. The blanking velocities investigated are initiated by moving the die based on measured velocity profiles, whereas the blanking punch is fixed in space. Die, blanking punch, blank holder, counter punch and blank were meshed as 3D bodies with tetrahedral elements. To evaluate the meshing quality, a mesh convergence analysis was carried out based on averaged temperature and stress values in the defined measuring fields of the shear zone. At a minimum edge length of 0.35 mm, the temperature and stress values converged with sufficient accuracy. In the area of the punch surfaces and blanking edges on the die, the elements were therefore meshed with a minimum edge length of l_E = 0.3 mm both in the sheet metal blank as well as in the contact area of the corresponding tool elements. With increasing distance from the contact surfaces as well as blanked part area, the minimum edge length was increased in two steps to $l_\mathrm{E} \approx$ 1.2 mm, so that in each case there is a size difference of factor two to neighboring volume elements. All tool elements were modeled elastically for realizing thermally coupled material behavior. Table 2 shows the physical and thermophysical parameters used for die and blanking punch (Böhler S390) as well as blank holder and counter punch (cold work tool steel X155CrVMo12-1 or 1.2379).

Table 2: Parameters used for Young's modulus E, Poisson's ratio ν, Density ρ, Thermal conductivity λ, Specific heat capacity c, Coefficient of thermal expansion a at 20 °C regarding the tool elements (die, blanking punch, blank holder, counter punch)

Material	E / GPa	ν / -	ρ / kg/m³	λ / W/(m·K)	c / J/(kg·K)	a / 10⁻⁶/K
Böhler S390	231	0.285	8100	17	420	10
1.2379	218	0.285	7680	29.2	465	10.1

The material behavior of the sheet metal material 42CrMo4+AC was modeled thermoviscoplastically using a remeshing algorithm. The flow behavior was modeled temperature and strain rate dependent according to Hensel and Spittel (1978) using model parameters of Landolt-Börnstein database (Spittel and Spittel (2009)). Equation 1 gives the parameters used for modeling the true stress σ_f as a function of temperature ϑ, true strain $\varphi = \varepsilon_\mathrm{pl}$ and strain rate $\dot{\varphi}$.

$$\sigma_\mathrm{f}(\vartheta, \varphi, \dot{\varphi}) = 929.822 \cdot e^{-0.00064 \cdot \vartheta} \cdot \varphi^{0.08896} \cdot \dot{\varphi}^{0.01142} \cdot e^{-0.00802/\varphi} \text{ MPa} \quad (1)$$

Except for the used Poisson's ratio of ν = 0.285, the physical as well as thermophysical parameters of 42CrMo4+AC were modeled temperature dependent in the range of 20 to 400 °C (Table 3).

Table 3: Temperature dependent parameters used for Young's modulus E, Density ρ, Thermal conductivity λ, Specific heat capacity c, Coefficient of thermal expansion a regarding the sheet metal material 42CrMo4+AC according to Spittel and Spittel (2009) as well as Richter (2011)

Temperature ϑ / °C	E / GPa	ρ / kg/m³	λ / W/(m·K)	c / J/(kg·K)	a / 10⁻⁶/K
20	212	7818.7	40.38	475.18	10.79
100	207	7792.3	42.36	488.62	11.23
200	199	7762.5	42.33	502.02	11.98
300	192	7730.4	40.50	522.15	12.54
400	184	7696.1	38.00	546.61	13.06

In order to consider deletion of elements during the shearing process and an associated thermal influence on the shear zone, the Cockcroft-Latham normalized ductile fracture criterion C_CL modified by Oh et al. (1979) was used. The criterion (Equation 2) is based on the maximum principal stress σ_max, the equivalent stress $\bar{\sigma}$ and the equivalent true or plastic strain at fracture $\bar{\varphi}_\mathrm{f}$. Elements are deleted when the computed fracture criterion reaches the defined critical fracture threshold C_crit.

$$C_\mathrm{CL} = \int_0^{\bar{\varphi}_\mathrm{f}} \frac{\sigma_\mathrm{max}}{\bar{\sigma}} \mathrm{d}\bar{\varphi} \quad \text{with element deletion at } C_\mathrm{CL} \geq C_\mathrm{crit} \quad (2)$$

Based on the investigations of Wai Myint et al. (2018), an interpolated value of $C_{\mathrm{crit}} = 1.44$ has been assumed for the critical ductile fracture regarding the die clearance of 0.4% relative to the sheet thickness used in this work. The friction between the sheet metal material and the tool elements was modeled using a Coulomb friction law limited by the shear friction law (e.g. in Klocke (2013)) with a friction coefficient of $\mu = 0.1$ and a shear factor of $m = 0.2$ at high contact normal stresses.

For considering the influence of high contact normal stresses in the area of the die and punch edges on the contact heat transfer under steady-state modeled conditions, a partitioning of two different areas for the contact heat transfer coefficient h_{ci} was performed (Fig. 2b). Depending on determined contact normal stresses during fine blanking, h_{c1} describes the contact heat transfer in the area of the die as well as punch edges and h_{c2} that on the remaining contact surfaces. According to the work of Rosochowska et al. (2003), at expected maximum shear temperatures of 200 to 300 °C and considering the contact normal stresses as well as surface roughness, for the partitions values of $h_{\mathrm{c1}} >$ 400 kW/(m²·K) and for h_{c2} of 100 to 300 kW/(m²·K) were assumed. Based on the thermographically determined sheared surface temperatures, an iterative approach was used at medium blanking velocity (45 mm/s) to numerically determine a value of 800 kW/(m²·K) for h_{c1} and a value of 200 kW/(m²·K) for h_{c2}. The numerical simulation sequence was conducted in two steps (Fig. 2b) with an initial material as well as ambient temperature of 20 °C. In the first step, the shearing process during fine blanking up to the time of ejection t_{eject} was simulated with the setup shown in Fig. 2a. In order to couple the sheared surface temperatures determined by thermography, the second step was to simulate the heat equalization processes between the blanked part and the counter punch as well as the environment, whereby the convective heat transfer between air and steel was modeled with value of $h_{\mathrm{conv}} = 10$ W/(m²·K). To model the thermal radiation, a value of $\varepsilon_{\mathrm{r}} = 0.24$ was used for the emissivity of bright steel surfaces.

The thermomechanical coupling is based on the differential equation for heat (Equation 3) according to Fourier. The coupling of the heat equation with continuum mechanics as well as the underlying numerical method of solution modeled in Forge is described in detail in Chenot and Bellet (1992) as well as Chenot et al. (1998).

$$\rho c \, \frac{\mathrm{dT}}{\mathrm{d}t} = \; \mathrm{div}\big(k \, \mathrm{grad}(T)\big) + \dot{q}_{\mathrm{vp}} \tag{3}$$

The heat equation describes the time derivative $\mathrm{d}t$ of the temperature T, considering the density ρ and specific heat capacity c. The right-hand side of the differential equation is divided into a surface and volume term. The latter represents the strain energy $\dot{q}_{\mathrm{vp}}$, which dissipates into heat due to viscoplastic deformation and results from the plastic strain energy $\dot{w}_{\mathrm{pl}}$ (Equation 4).

$$\dot{q}_{\mathrm{vp}} = r \cdot \dot{w}_{\mathrm{pl}} = r \cdot \boldsymbol{\sigma} : \dot{\boldsymbol{\varepsilon}} \qquad \text{with } 0.9 \le r \le 1 \text{ and in general } \dot{\boldsymbol{\varepsilon}} = \dot{\boldsymbol{\varepsilon}}_{\mathrm{el}} + \dot{\boldsymbol{\varepsilon}}_{\mathrm{pl}} \text{ (elastic and plastic part)} \tag{4}$$

The factor r describes the thermal efficiency (here 0.9) and considers the proportion of dislocation energy in the plastic strain energy. The plastic strain energy $\dot{w}_{\mathrm{pl}}$ is generally determined by a double contracted product of the stress tensor $\boldsymbol{\sigma}$ and the strain rate tensor $\dot{\boldsymbol{\varepsilon}}$. The surface term (Equation 5) with the thermal conductivity k and normal of the surface $\boldsymbol{n}$ in general describes the heat flux at the contact surfaces between tool and sheet metal as well as the free surfaces with the environment (Ripert et al. (2015)). For the heat transfer at the contact surfaces, conduction as well as dissipated energy of the frictional shear stress $\boldsymbol{\tau}_{\mathrm{fr}}$ are modeled, considering the thermal effusivity of the tool b_{tool} and sheet metal material b as well as the relative velocity $\boldsymbol{v}_{\mathrm{rel}}$ between tool and sheet metal.

$$-k \, \mathrm{grad}(T) \cdot \boldsymbol{n} = \begin{cases} h_{\mathrm{ci}} \, (T - T_{\mathrm{tool}}) - \frac{b}{b + b_{\mathrm{tool}}} \, \boldsymbol{\tau}_{\mathrm{fr}} \cdot \boldsymbol{v}_{\mathrm{rel}} \\ h_{\mathrm{conv}} \, (T - T_{\mathrm{amb}}) \; + \; \varepsilon_{\mathrm{r}} \, \sigma_{\mathrm{r}} \, (T^4 - T_{\mathrm{amb}}^4) \end{cases} \qquad \text{with } b_i = \sqrt{k_i \, \rho_i \, c_i} \text{ and } \boldsymbol{v}_{\mathrm{rel}} = \boldsymbol{v} - \boldsymbol{v}_{\mathrm{tool}} \tag{5}$$

The heat transfer with the environment at the free surfaces is modeled by natural convection with the ambient temperature T_{amb} as well as thermal radiation, where σ_{r} denotes the Stefan-Boltzmann constant.

3. Result analysis

Fig. 3a shows the influence of the investigated blanking velocity on the experimentally and numerically determined temperature distribution of the sheared surface when reaching the bottom dead center (BDC) at t_{BDC} ($t = 0$ s). Independent of the blanking velocity, the highest temperatures occur at the corner areas of the blanked part geometry

due to locally high deformation during the shearing process, frictional influences as well as the local overlapping of heat flows of neighboring sheared surface areas. With rising blanking velocity, a significant temperature increase can be observed both at the corner areas as well as of the sheared surface temperature T_S averaged in the measuring fields. The visualized temperature distribution of the respective measuring fields is relatively homogeneous within the defined temperature ranges, which is more uniformly pronounced in the numerical results. The comparison between numerically calculated and thermographically determined sheared surface temperature shows a sufficiently accurate correspondence in the depicted temperature progression with differences of 1 to 2 °C for all blanking velocities (Fig. 3b). However, for the thermographically determined sheared surface temperatures below 45 °C, possible deviations have to be considered due to the proximity to the prevailed ambient temperature of approx. 20 °C as well as the radiation properties of smooth and bright metallic surfaces at these temperatures.

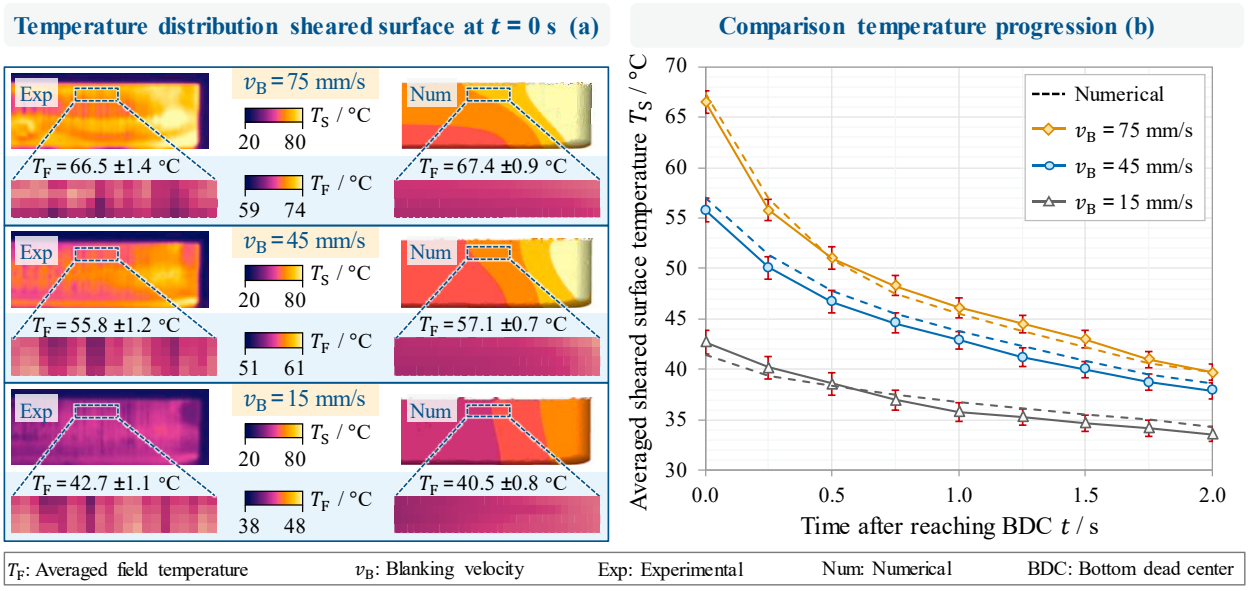


Fig. 3: Determined temperature distribution on the sheared surface when reaching the BDC (a) as well as the resulting temperature progression (b)

Fig. 4a and b exemplarily show the progression of the experimentally and numerically determined blanking force F_B as well as blanking work W_B for low (15 mm/s) and high (75 mm/s) blanking velocity v_B as a function of the shearing path z_S. The not shown force as well as work progression at medium blanking velocity (45 mm/s) lies in each case between the values of low and high velocity and thus verifies the emerging tendency. Compared to high, the low blanking velocity leads to a slight increase of the averaged maximum blanking force $F_{B,max}$ of about 1.7% regarding the experimental values and about 2.1% regarding the numerical ones. Clearly more pronounced is the difference between the areas of the respective blanking force curves, which was quantified by means of the blanking work using numerical integration based on the trapezoidal rule. An increasing blanking velocity results in a significant reduction of the cumulative blanking work $W_{B,c}$ over the shearing path of about 8.7% regarding the experimental values and about 3.7% regarding the numerical ones. Experimentally and numerically determined blanking force as well as work show qualitatively a comparable progression. However, in the elastic range at the beginning of the shearing process ($z_S \leq 0.5$ mm) and with decreasing cross section of the sheet metal material to be separated towards the end of the shearing process ($z_S > 2.5$ mm), the experimental blanking force curves differ from the numerical ones. The experimental blanking force rises less steeply in the elastic range and falls with a smaller gradient after reaching the maximum, whereby the latter is much more pronounced at low blanking velocity. In addition, towards the end of the experimental blanking force curve ($z_S \approx 4.8$ to 5.2 mm), an abrupt separation of the remaining cross section can be observed. Possible causes for the less steep elastic rise at the beginning as well as the less steep decrease after reaching the maximum of the experimental blanking forces are elasticities in the structure of the fine blanking press and tool as well as moments of inertia of the press ram kinematics and the dynamic effects coupled with them, which are not

sufficiently represented by the numerical model setup. The experimentally observed abrupt separation to the end of shearing is due to stored elastic energies in the structure of the fine blanking press and tool, which was verified by means of investigations with a digital contact sensor.

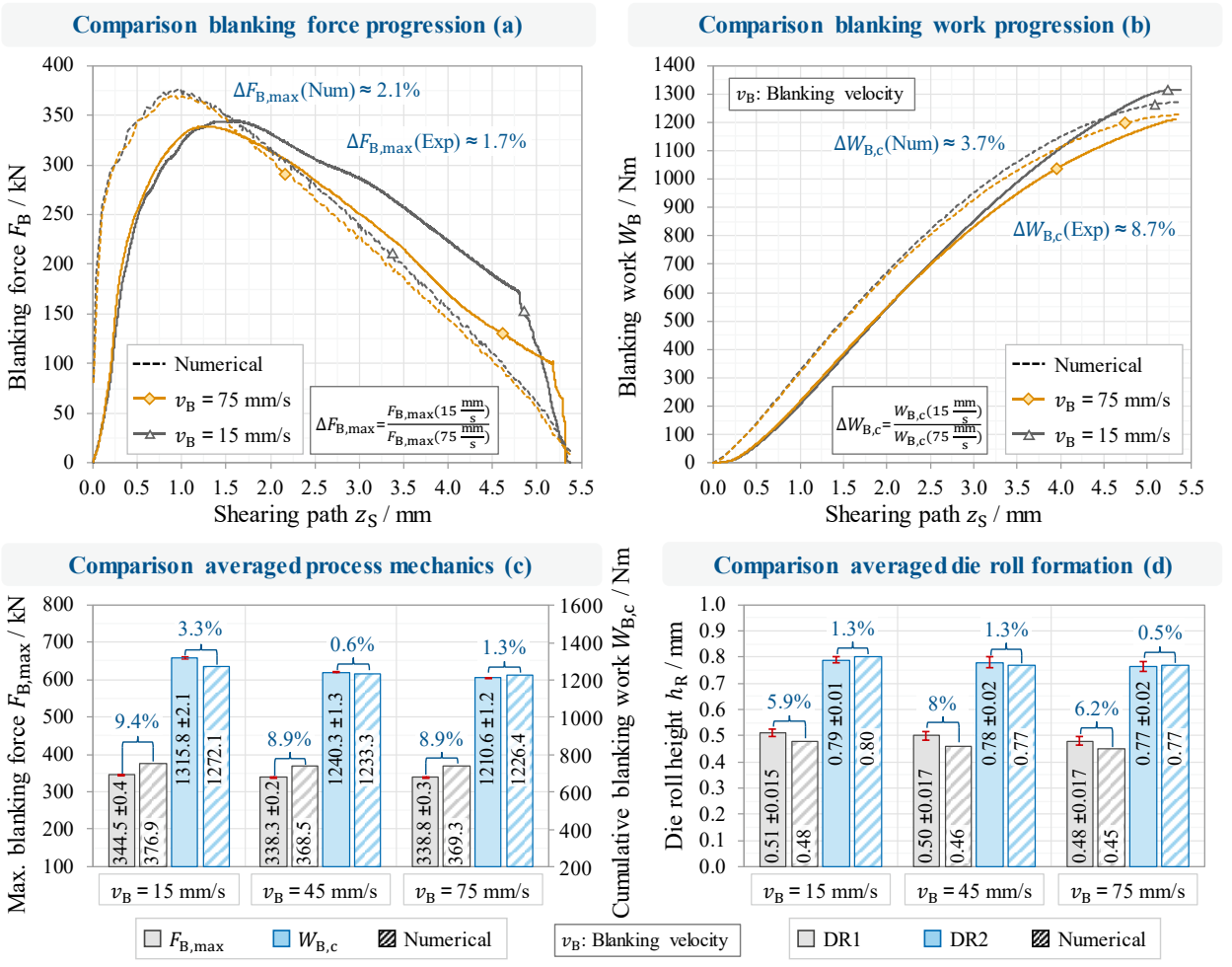


Fig. 4: Comparison of blanking force (a) and work (b) progression with averaged maxima (c) as well as averaged die roll height (d)

The numerically calculated maximum blanking forces are about 9% higher than the experimentally determined ones (Fig. 4c), which is due to strength differences between the used flow curve parameters from the database and the experimentally used quenched and tempered steel. The comparison between the experimentally averaged and numerically calculated die roll height h_R shows smaller deviations for the corner areas (DR2) with approx. 1% than for the side areas (DR1) with 6 to 8% (Fig. 4d). However, regarding the meshed element size, the numerical mapping of the die roll is to be evaluated as sufficiently accurate.

For numerical analysis regarding the influence of the blanking velocity on the shear zone temperature T_{SZ}, the area with respect to the center of the defined measuring field was evaluated. Fig. 5a shows the temperature distribution at the highest shear zone temperature that occurred in each case in relation to the shearing path z_S. With increasing blanking velocity, the temperature maximum is shifted towards the separation of the blanked part, which occurs at the top dead center (TDC) with $z_S \approx 5.4$ mm (5 mm sheet thickness + 0.3 mm chamfer height + 0.1 mm immersion depth). The temperature distribution reveals a significant increase in shear zone temperature due to increased blanking velocity. In order to quantify the progression of the shear zone temperature as a function of the shearing path, several elements in the area of the die chamfer were averaged in relation to the center of the defined measuring field (Fig. 5b).

Starting from low blanking velocity (15 mm/s), the shear zone temperature increases from about 146 °C to 260 °C at high velocity (75 mm/s) in the evaluated measuring field. The maximum calculated shear zone temperatures (dash lines) are outside the measuring field and approx. 10 °C higher in each case.

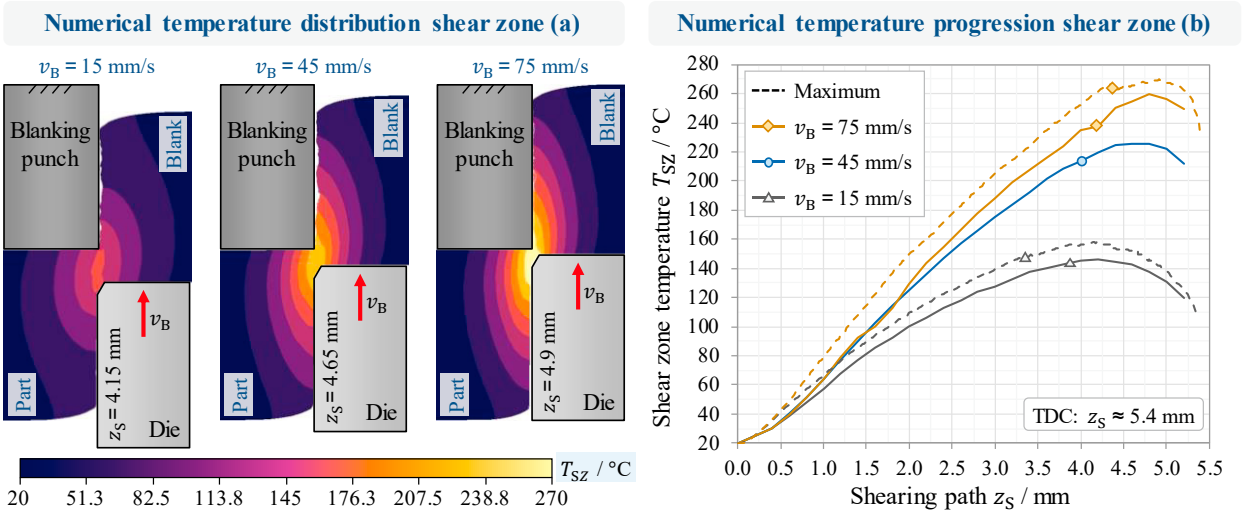


Fig. 5: Temperature distribution when reaching the maximum (a) as well as temperature progression depending on the shearing path (b)

4. Discussion and conclusion on thermomechanical modeling of the shearing process

For thermomechanically coupled FE modeling of the shearing process during fine blanking, the contact heat transfer was calibrated using thermographically determined sheared surface temperatures. The sheet metal material was modeled using a thermoviscoplastic flow curve model and, with exception of the Poisson's ratio, temperature-dependent physical as well as thermophysical parameters. A partitioning of two areas for contact heat transfer allowed local adaptation considering the prevailing conditions. The use of results from the literature enabled an iterative calibration of the contact heat transfer coefficients, considering the contact normal stresses, surface roughness as well as expected shear zone temperatures. For evaluation, Table 4 shows the influence of the investigated ranges of contact heat transfer coefficients h_{ci} on the numerically calculated temperatures related to the iteratively determined values (Ref) of h_{c1} = 800 kW/(m²·K) and h_{c2} = 200 kW/(m²·K) at medium blanking velocity (45 mm/s).

Table 4: Influence of varied contact heat transfer areas on the maximum shear zone temperature $T_{SZ,max}$ as well as the sheared surface temperature before ejection T_{eject}, each related to the iteratively determined reference state (Ref in blue) for a blanking velocity of 45 mm/s

h_{c1} / kW/(m²·K)	800	800	800	400	1200
h_{c2} / kW/(m²·K)	50	100	300	200	200
$T_{SZ,max}(h_{c1/2})/T_{SZ,max}$(Ref)−1 / %	4.3	1.1	-0.5	0.7	-1.4
$T_{eject}(h_{c1/2})/T_{eject}$(Ref) −1 / %	5.8	2.9	-1.8	0.3	-0.5

A reduction of the contact heat transfer coefficient leads to an increase of the numerically calculated temperatures due to reduced heat transfer. The most significant influence on the shear zone or sheared surface temperature is caused by the partitioned contact area regarding h_{c2}. A possible explanation for this is the relatively small number of contact points in terms of heat transfer regarding h_{c1} at the die as well as punch edges due to the meshed element size used. However, both partitions combined increase the influence of the modeled contact heat transfer on the heat equalization processes, which enables larger calibration ranges. In addition, reducing the value for critical ductile fracture to C_{crit} = 1 resulted in a 0.8% decrease and increasing it to C_{crit} = 2 in a 0.2% increase in the maximum shear zone

temperature $T_{SZ,max}$. A temperature-independent modeling of the physical and thermophysical parameters of the sheet metal material with constant values for 20 °C resulted in an increase of the maximum shear zone temperature of 2.7 %.

Calibration of the thermomechanically coupled FE model using thermographically measured sheared surface temperatures after fine blanking showed a sufficiently accurate correspondence of the temperature progressions. Regardless of the time differences between TDC and BDC, a significant temperature increase of about 25 °C on the sheared surface is evident as a result of a 60 mm/s increase in blanking velocity. Compared to the numerical blanking force curves, the experimentally determined force progressions showed a less steep elastic rise and a lower falling gradient towards the end of the shearing process. Process-related high loads during fine blanking result in elastic deformation of the knuckle joint system of the servomechanical press ram drive as well as the force-transmitting pressure pins for the counter and blank holder force. Due to the elastic deformation, the force transmission elements of the press ram drive and tool are compressed in shearing direction, which leads to a delayed linear increase in blanking force in the real process compared to the numerically determined increase in force. This elastic upsetting of the force transmission elements is at least partially maintained after the maximum blanking force is reached until the sheet metal material is separated, which explains the smaller falling gradient of the experimental force progression. At the end of the shearing process, the stored elasticity is released analogous to a spring in shearing direction, which leads to an abrupt separation of the remaining cross section of the sheet metal material (Fig. 4a almost vertically decreasing force curve). This abrupt separation is possible because the hydraulically applied counter force is depressurized on the press side when TDC is reached until the blanked part is ejected. Regarding the significant difference in the falling range of the experimental blanking force progression at low blanking velocity and the associated higher experimental blanking work, dynamic effects due to the moments of inertia of the press ram are to be assumed, which are not represented by the numerical model setup.

Numerical analysis of the shear zone temperature revealed a significant increase in the maximum shear zone temperature occurring along the shearing path with increasing blanking velocity, which is in agreement with experimentally determined results of Demmel et al. (2015). Higher blanking velocities reduce the time available for heat equalization processes and thus cause an increased accumulation of dissipated heat in the area in front of the die as well as punch edges, as evidenced by the visualized numerical temperature distributions. As a result of increased heat accumulation, thermal softening of the sheet metal material in the shear zone is to be expected, which at least partially explains the reduction in blanking work with increasing blanking velocity. The relative difference between the numerically and experimentally determined blanking work can be attributed to the elastic work required during the process-related deformation of the force transmission elements of the press ram drive and tool as well as possible dynamic effects in the real process. In summary, the following conclusions are derived:

- Temperature-dependent physical and thermophysical parameters as well as the ductile fracture criterion reduce the maximum calculated shear zone temperatures of the thermoviscoplastic material model used and should therefore be considered.
- If accurate values regarding the contact heat transfer coefficient are not available, the determination of thermography-based sheared surface temperatures offers a possibility to calibrate the contact conditions during the shearing process. Partitioning for assumed steady-state contact heat transfer areas represents a simplified approach to consider locally varying contact normal stresses in the shear zone.
- The blanking work required includes the process-related elastic deformation of the force transmission elements of the servomechanical press ram drive as well as the fine blanking tool. These elastic deformations need to be considered for a more detailed numerical process model.
- Based on calibrated contact conditions, numerically calculated temperature distributions in the shear zone enable an analysis of the influence of process parameters on material behavior during the shearing process and thus support material as well as process design for fine blanking.

Acknowledgements

The authors would like to thank the German Research Foundation (DFG) for founding this research under the project number 520460745 within the priority program SPP 2422.

References

Babaei, S.N., Schweinshaupt, F., Wipp, S., Herrig, T., Krupp, U., Bergs, T., 2023. Mechanism-driven fine blanking of high manganese steels. Journal of Materials Processing Technology 319, https://doi.org/10.1016/j.jmatprotec.2023.118083.

Chenot, J.-L., Bellet, M., 1992. The Viscoplastic Approach for the Finite-Element Modelling of Metal-Forming Processes. In: Hartley, P., Pillinger, I., Sturgess, C. (Eds.) Numerical Modelling of Material Deformation Processes. Springer London, London, pp. 179–224, https://doi.org/10.1007/978-1-4471-1745-2_8.

Chenot, J.-L., Fourment, L., Coupez, T., Ducloux, R., Wey, E., 1998. Forge3 (R) - a general tool for practical optimization of forging sequence of complex three-dimensional parts in industry. International Conference on Forging and Related Technology (ICFT 98), 113–122.

Demmel, P., Hoffmann, H., Golle, R., Intra, C., Volk, W., 2015. Interaction of heat generation and material behaviour in sheet metal blanking. CIRP Annals 64, 249–252, https://doi.org/10.1016/j.cirp.2015.04.091.

Hensel, A., Spittel, T., 1978. Kraft- und Arbeitsbedarf bildsamer Formgebungsverfahren: Mit 51 Tabellen, 1st ed. Dt. Verl. für Grundstoffindustrie, Leipzig, 528 S.

Joun, M.-S., Razali, M.K., Jee, C.-W., Byun, J.-B., Kim, M.-C., Kim, K.-M., 2022. A Review of Flow Characterization of Metallic Materials in the Cold Forming Temperature Range and Its Major Issues. Materials (Basel, Switzerland) 15, https://doi.org/10.3390/ma15082751.

Kim, S.-H., Kang, J., Lee, D.-J., Lee, K.-Y., Kim, H.-Y., Kim, H.-J., 2007. The Effect of Temperature Rise in a Fine Blanking Tool, in: AIP Conference Proceedings. MATERIALS PROCESSING AND DESIGN; Modeling, Simulation and Applications; NUMIFORM '07; Proceedings of the 9th International Conference on Numerical Methods in Industrial Forming Processes, Porto (Portugal), pp. 877–882, https://doi.org/10.1063/1.2740921.

Klocke, F., 2013. Manufacturing Processes 4: Forming. Springer Berlin Heidelberg, Berlin, Heidelberg.

Kolhatkar, A., Pandey, A., 2023. Sheet Metal Shearing Process: An Overview. Trans Indian Natl. Acad. Eng. https://doi.org/10.1007/s41403-023-00421-y.

Oh, S.I., Chen, C.C., Kobayashi, S., 1979. Ductile Fracture in Axisymmetric Extrusion and Drawing — Part 2: Workability in Extrusion and Drawing. Journal of Engineering for Industry 101, 36–44, https://doi.org/10.1115/1.3439471.

Richter, F., 2011. Die physikalischen Eigenschaften der Stähle - Das 100-Stähle-Programm. https://www.tugraz.at/fileadmin/user_upload/Institute/IEP/Thermophysics_Group/Files/Staehle-Richter.pdf. Accessed 17 September 2023.

Ripert, U., Fourment, L., Chenot, J.-L., 2015. An upwind least square formulation for free surfaces calculation of viscoplastic steady-state metal forming problems. Adv. Model. and Simul. in Eng. Sci. 2, https://doi.org/10.1186/s40323-015-0037-5.

Rosochowska, M., Balendra, R., Chodnikiewicz, K., 2003. Measurements of thermal contact conductance. Journal of Materials Processing Technology 135, 204–210, https://doi.org/10.1016/S0924-0136(02)00897-X.

Spittel, M., Spittel, T., 2009. Steel symbol/number: 42CrMo4/1.7225. In: Martienssen, W., Warlimont, H. (Eds.) Metal Forming Data of Ferrous Alloys - deformation behaviour, 2C1. Springer Berlin Heidelberg, Berlin, Heidelberg, pp. 1050–1055, https://doi.org/10.1007/978-3-540-44760-3_166.

Wai Myint, P., Hagihara, S., Tanaka, T., Taketomi, S., Tadano, Y., 2018. Application of Finite Element Method to Analyze the Influences of Process Parameters on the Cut Surface in Fine Blanking Processes by Using Clearance-Dependent Critical Fracture Criteria. JMMP 2, 26, https://doi.org/10.3390/jmmp2020026.